

# Self-referenced coherent diffraction x-ray movie of Ångstrom- and femtosecond-scale atomic motion

J. M. Gownia,<sup>1,2,\*</sup> A. Natan,<sup>1,\*</sup> J. P. Cryan,<sup>1</sup> R. Hartsock,<sup>1</sup> M. Kozina,<sup>2</sup> M. P. Miniti,<sup>2</sup> S. Nelson,<sup>2</sup> J. Robinson,<sup>2</sup> T. Sato,<sup>2</sup> T. van Driel,<sup>2</sup> G. Welch,<sup>2</sup> C. Weninger,<sup>1,2</sup> D. Zhu,<sup>2</sup> and P. H. Bucksbaum<sup>1,3</sup>

<sup>1</sup>Stanford PULSE Institute, SLAC National Accelerator Laboratory Menlo Park, CA 94025

<sup>2</sup>Linac Coherent Light Source, SLAC National Accelerator Laboratory, Menlo Park, CA 94025

<sup>3</sup>Departments of Physics, Applied Physics, and Photon Science, Stanford University, Stanford, CA 94305.

(Dated: October 31, 2018)

Time-resolved femtosecond x-ray diffraction patterns from laser-excited molecular iodine are used to create a movie of intramolecular motion with time and space resolution of 30 fs and 0.3 Å. The high spatial fidelity is due to interference between the moving excitation and the static initial charge distribution. This x-ray interference has not been employed to image internal motion in molecules before. The initial state is used as the local oscillator for heterodyne amplification of the excited charge distribution to retrieve real-space movies of atomic motion on Ångstrom and femtosecond scales. Coherent vibrational motion and dispersion, dissociation, and rotational dephasing are all clearly visible in the data, thereby demonstrating the stunning sensitivity of heterodyne methods.

High brightness ultrafast hard x-ray free electron lasers (FELs) can perform time-resolved x-ray diffractive imaging. Recent demonstrations of time-resolved crystal diffraction or time-resolved non-periodic imaging illustrate the power of these sources to track Ångstrom-scale motion. [1, 2]. These have spurred new insights in broad areas of science, but have not fully realized the potential of x-ray FELs to image molecules with simultaneous sub-Ångstrom and few-femtosecond resolution. Attempts to achieve this show correlations between predicted and observed x-ray scattering. [3, 4]. These studies relied on simulations to extract molecular dynamics from the scattering data.

Here we propose and demonstrate an imaging method that employs a universal and unappreciated feature of time-resolved hard x-ray scattering that dramatically improves reconstructed images of charge motion, and enables femtosecond and sub-Ångstrom x-ray movies. The method relies on the “pump-probe” protocol, where motion is initiated by a short “start” pulse, and then interrogated at a later time by a “probe” pulse. The pumped fraction is small, i.e. most of the molecules are not excited, and this produces our heterodyne reference.

When a gas of  $N$  identical molecules in a thermal distribution is excited with probability  $a$  from the ground state  $g$  to an excited state  $e$ , only a fraction  $aN$  molecules are in  $e$  but there is no information about which ones. If we scatter x-rays from this system, the elastic scattering amplitude  $f(\vec{Q})$  is the normalized sum of  $f^{(g)}$  or  $f^{(e)}$  from all  $N$  molecules in all  $M$  possible excitation configurations where  $M = \binom{N}{aN} = N! / [(N - aN)!aN!]$ .

$$f(\vec{Q}) = (1/M) \sum_{i=1}^M \left[ \sum_{j=1}^{aN} f_{ij}^{(e)}(\vec{Q}) + \sum_{j=1}^{(1-a)N} f_{ij}^{(g)}(\vec{Q}) \right]. \quad (1)$$

The order of summing can be re-arranged so that the

factor  $1/M$  cancels the sum over  $i = 1, M$ , leaving:

$$f(\vec{Q}) = \sum_{j=1}^N [af_j^{(e)} + (1 - a)f_j^{(g)}] \quad (2)$$

The square of this amplitude is the intensity on the detector. Cross terms between different molecules average out due to their random position in the gas, so the scattered intensity  $I$  is linear in the number of molecules  $N$ :

$$I(\vec{Q}) = |f(\vec{Q})|^2 = N|af^{(e)} + (1 - a)f^{(g)}|^2 \quad (3)$$

This signal is an incoherent sum of the coherent diffraction from each molecule as defined later in Eq. 5. Such a system is described by a quantum density matrix for coherent rovibrational excitation with incoherent mixtures of ground and excited electronic states.

The key insight in Eq. 3 is that x-ray scattering from the excited fraction in each molecule interferes with scattering from its initial state fraction, producing holographic fringes. Previous descriptions of the formal theory of time-resolved x-ray diffraction in small molecules have not discussed the importance of this self-referenced interference [5–12]. Eq. 3 has been noted previously, but has not been implemented for molecular movies [12–15].

Even when only 1% of the ensemble is excited, the excited state features have sufficient visibility to be seen in the raw data due to holographic interference, and simple heterodyne deconvolution methods can extract an image of the moving charge. The initial state charge distribution can in principle be extracted from the portion of the data set collected at negative pump-probe delays, when the probe pulse is only interacting with the initial state. The deconvolved signal is a real-space *de-novo* molecular movie.

A demonstration of coherent self-referenced time-resolved imaging with  $\sim 30$  fs and  $\sim 0.3\text{\AA}$  resolution was performed at the X-ray Pump Probe (XPP) facility

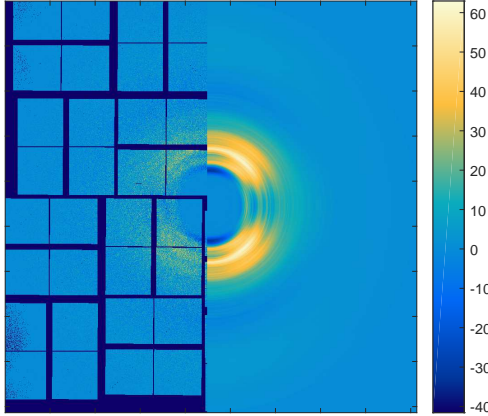


FIG. 1. Left: Half of the CSPAD showing diffraction at a pump-probe delay of 750 fs, with the time-averaged image subtracted. Right: Half of Legendre fit scattering pattern of Eq. 4 at the same time delay, also with time-averaged image subtracted.

at the Linac Coherent Light Source (LCLS) [16]. The apparatus for gas phase scattering has been described previously [17]. Briefly, the pump pulse ( $520 \pm 5$  nm, 0.1 mJ, 120 Hz, 50 fs, vertical polarization) was created through frequency mixing of signal (1486 nm) and pump (800 nm) laser radiation from an optical parametric amplifier (OPA, Coherent OperA Solo). The probe pulse (9.0 keV, 2 mJ, 120 Hz, 40 fs, horizontal polarization) was a highly spatially coherent beam of x-rays provided by the LCLS. The beams were both focused into a windowless iodine cell inside a larger vacuum enclosure with a sapphire/beryllium output window. The cell was heated to  $100^\circ$  C, providing 45 Torr vapor pressure with a column density of  $\sim 10^{18}$  cm $^{-2}$  and an X-ray attenuation of 8%. X-ray photoabsorption, though present at these x-ray energies, does not affect the fidelity because of the “diffract-before-destroy” principle. The scattered x-rays were detected by a CSPAD 2.3 megapixel detector [18].

A typical diffraction pattern for  $\sim 100$  pulses is shown in Fig. 1. These data have been discriminated based on x-ray beam parameters (bunch charge, photon energy, pulse energy, and beam position) and the average scattering over all delays has been subtracted. We remove the angle-dependent Thomson scattering effect due to horizontally polarized x rays, and we rebin in  $(Q, \theta)$  coordinates. Data from each radial value are fit to a Legendre basis (Fig.1)

$$I(Q, \theta, t) = A(Q, t) \left[ 1 + \sum_{n=1}^3 \beta_{2n}(Q, t) P_{2n}(\cos(\theta)) \right] \quad (4)$$

Only the even Legendre functions are used because the

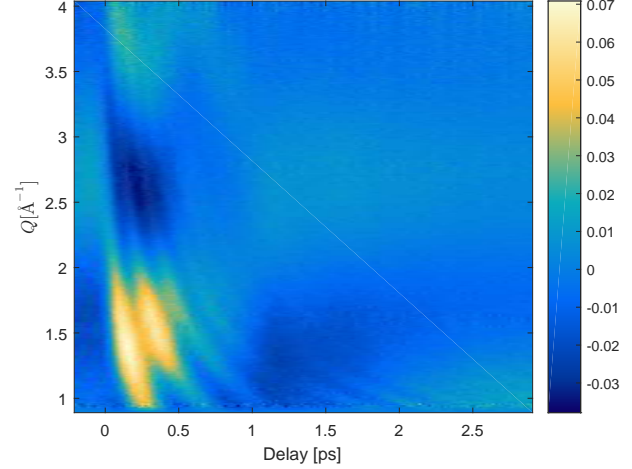


FIG. 2.  $\beta_2(Q, t)$  as defined in Eq. 4. This term captures most of the excited state scattering signal. The time-averaged value is subtracted for clarity. Long- (Short-) period Q-oscillations are due to holographic interference of the bound motion (dissociation) seen in Fig. 3.

geometry cannot break the up/down symmetry of the molecular ensemble. Contributions for  $n > 3$  are negligible.

The radial modulations in Fig. 1 are captured in the  $\beta_2(Q, t)$  coefficient of Eq. 4, plotted in Fig. 2. This picks out scattering patterns with the symmetry of an electric dipole excitation, and contains nearly all of the time-varying portion of the total scattered signal. The large-amplitude modulations in Fig. 2 are due to holographic interference between the charge distribution of the laser-excited wavepacket and the static ground state. Heterodyne techniques described below allow us to deconvolve the excitation in space and plot it vs. time in Fig. 3 as a movie with femtosecond and Ångstrom resolution.

For time delays  $t < 0$  the x-rays scatter from the iodine before the exciting laser arrives in the sample, and therefore the distribution is static and contained in the isotropic  $A(Q, t)$  portion of Eq. 4.

The features in the movie that follow the excitation pulse at  $t=0$  reveal the detailed quantum evolution of this system. The letters at the beginning of the following paragraphs refer to labeled areas of Fig. 3.

(a) A region of approximately 100 fs (about five discrete pump-probe delay points) around  $t = 0$  shows where the excited state activity begins. The Franck Condon region, where the B-state is directly over the X-state, is centered around  $2.7 \text{ \AA}$  in iodine. Charge appears across this region moving rapidly towards the center of the B-state potential at approximately  $3 \text{ \AA}$  and then moving beyond towards the outer turning point, approximately  $4.5 \text{ \AA}$  for this excitation wavelength.

(b) The vibrational oscillations in bound states in the molecule can be observed in some detail. The retrieved

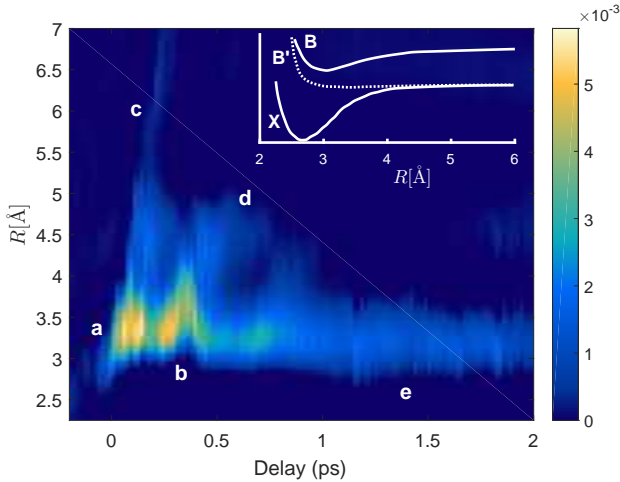


FIG. 3. Extracted excited-state charge distribution vs time, for  $R$  from 2.3 to 7 Å and time delays out to 2 ps. This “movie” was made from  $\beta_2(Q, t)$  (see Fig. 2) via the procedure in Eqns. 5-9. Bound-state wavepacket oscillations, dissociation, and rotational dephasing are clearly visible. Letters refer to molecular motion described in the text. Inset: Relevant interatomic potentials in diatomic iodine.

charge density and range of oscillation periods is consistent with bound coherent vibrations in the B-state following excitation by a 510-520 nm photon. The excitation is spread over several hundred  $\text{cm}^{-1}$  by thermal broadening of the initial state. In addition, the excited state wave packet is located high up in the anharmonic portion of the B-state potential well. These conditions lead to strong dispersion, which smears the outer turning point in both space and time. The precise location of the charge in the Fig. 3 also depends on the distribution of the bond axis alignment as discussed below.

(c) There is a pulse of dissociating charge that starts near  $(R, t) = (2.7 \text{ \AA}, 0)$  and moves rapidly away from the bound region with constant velocity and only 4% of the total excited charge. The fringes recorded in Fig. 2 are sufficiently fine to show that this feature has little dispersion out to at least 16 Å, well beyond the range included in Fig. 3. Its velocity is 16 Å/ps, corresponding to a kinetic energy release of approximately 0.85 eV, consistent with the separation velocity required for the molecule to dissociate into two ground-state atoms for our excitation wavelength. This prompt dissociation is consistent with transitions to a family of repulsive *ungerade* states, one of which is shown in the inset in Fig. 3.

(d) Local moving peaks in the charge density are observed near the outer turning point at time delays of 0.5-0.7 ps. Similar cusp-like features have been predicted for wave packets evolving in the highly dispersive upper parts of the B-state, but they have not been observed directly before [19].

(e) The width and mean value of the position of the

excited population gradually decreases for about 1.2 ps, reaching a minimum mean value near 3 Å. This is consistent with rotational dephasing of the initial alignment of the excited state. The excitation has a  $\cos^2 \theta$  alignment with laser polarization, but rotations of the thermal ensemble lead to dephasing with a rate that depends on temperature. For iodine at 100° C, we have calculated that the initial prolate alignment of the excited state fraction along the  $\hat{z}$  axis should evolve to a nearly isotropic distribution at 1.2 ps [20-22]. Our data in Fig. 3 agree with this prediction. Angular dephasing also affects the total amount of charge vs. time in Fig. 3. The amplitude decreases as population moves from  $\cos^2 \theta$  to a more isotropic distribution. Beyond the point of minimum alignment at 1.2 ps the signal is only about 1/3 the initial strength.

The method used to “invert” this scattering image uses the heterodyne beating between the excited and ground state that is evident in figure 2. Below we describe the step-by-step procedure for obtaining the movie in Fig. 3.

In x-ray diffraction the scattering amplitude  $f(\vec{Q})$  is a 2-dimensional Fourier transform of the instantaneous charge density,  $\rho(\vec{x}, t)$  [11]:

$$f(\vec{Q}, t) = \int d^3x \rho(\vec{x}, t) e^{i\vec{Q} \cdot \vec{x}} \quad (5)$$

where  $\vec{Q}$  is the photon momentum transfer. The charge density is concentrated on the iodine atoms and so the scattering depends primarily on their location within each molecule. Before excitation all of the iodine is in the ground X-state. The laser pulse creates rovibrational wavepackets on excited electronic states. A majority of the excited state population resides in the B-state. The much faster electronic coherence beats between the X and B state are averaged out.

The charge density  $\rho(\vec{x}, t)$  that appears in Eq. 5 is the expectation value of the charge density operator in the  $|\vec{x}\rangle$  basis, which is the trace of the density matrix over the electronic coordinates multiplied by the electron charge. This can be divided into an initial charge distribution  $\rho_0(\vec{x})$  and a time-varying distribution  $\rho_e(\vec{x}, t)$  without loss of generality. This agrees with Eq. 3 for the x-ray intensity  $I(\vec{Q}, t) = |f(\vec{Q}, t)|^2$ .

We approximate  $\rho_0(\vec{x})$  in the analysis by  $\rho(\vec{x}, t < 0)$ , the charge distribution before the laser excitation. The object of the analysis is to discover  $\rho_e(\vec{x}, t > 0)$ , and thereby create a molecular movie. The precise form of the time-independent initial distribution is easily calculated, but we stress here that its most important feature is that it serves as a time-independent reference in the time-varying scattering pattern in a pump-probe experiment.

The process of extracting the moving charge distribution from the measured scattering pattern follows the established lines of heterodyne deconvolution. The first step is to perform a 2-dimensional inverse Fourier trans-

form on the scattering image. This cannot recover the charge distribution directly because the scattering is the magnitude squared of the charge Fourier transform and therefore is a real function that has no phase information. However it does produce an autocorrelation of the charge distribution, which is a simple consequence of the convolution theorem:

$$\begin{aligned} \mathcal{FT}_{2D}^{-1}(f(\vec{Q}, t)f^*(\vec{Q}, t)) &= \mathcal{AC}[\rho(\vec{x}, t)] \\ &\equiv \rho(\vec{x}, t) \otimes \rho(\vec{x}, t) \end{aligned} \quad (6)$$

The right side of Eq. 6 can be expanded into the contributions from its time-independent reference and its smaller time-dependent wave packet:

$$\begin{aligned} \mathcal{AC}[\rho(\vec{x}, t)] &= \mathcal{AC}[\rho_0(\vec{x})] + \mathcal{AC}[\rho_e(\vec{x}, t)] \\ &\quad + 2\mathcal{CC}[\rho_0(\vec{x}), \rho_e(\vec{x}, t)] \end{aligned} \quad (7)$$

Here  $\mathcal{CC}$  is a convolution integral (i.e. cross-correlation)  $\mathcal{CC}[\rho_0(\vec{x}), \rho_e(\vec{x}, t)] = \rho_0(\vec{x}) \otimes \rho_e(\vec{x}, t)$ . The first term in Eq. 7 on the right side is obtained from the  $t < 0$  measurements and can be subtracted. The second term is second order in the excitation fraction, and may be neglected if the excitation fraction is small, which is the standard assumption for pump-probe experiments. We then obtain:

$$2\mathcal{CC}[\rho_0(\vec{x}), \rho_e(\vec{x}, t)] \simeq \mathcal{AC}[\rho(\vec{x}, t)] - \mathcal{AC}[\rho_0(\vec{x})] \quad (8)$$

The final step to produce a molecular movie uses the convolution theorem once more to extract  $\rho_e(\vec{x}, t)$ .

$$\rho_e(\vec{x}, t) = \mathcal{FT}_{2D}^{-1} \left[ \frac{\mathcal{FT}_{2D}(\mathcal{CC}[\rho_0(\vec{x}), \rho_e(\vec{x}, t)])}{\mathcal{FT}_{2D}(\mathcal{AC}[\rho_0(\vec{x})])} \right]. \quad (9)$$

In this step the initial charge distribution  $\rho_0(\vec{x})$  is approximated as the thermal population of levels of the  $X$ -state:

$$\rho_0(\vec{x}) \sim \rho_X(\vec{x}) = \sum_{v=0}^{\infty} \rho_v(\vec{x}) e^{-E_v/k_B T}. \quad (10)$$

This is a compact 2-dimensional point-spread function for deconvolution in Eq. 9. The image retrieval is thus similar to deblurring in microscopy. To obtain our molecular movie we project Eq. 8 onto  $P_2(\cos \theta)$  and perform a deconvolution (Lucy-Richardson) along  $R$ , yielding Fig. 3. We have found that this deconvolution is robust for several standard algorithms. More sophisticated deconvolution methods might lead to further improvement in image definition, but this procedure is sufficient to reveal the main features of the charge motion with resolution that is already comparable to the limits in  $Q$  imposed by our scattering geometry.

The method of data collection and image inversion described here is not limited to diatomic molecules, and can be applied to many small molecules in liquid or gas phase. Thymine photoprotection, retinal isomerization,

and cyclohexadiene ring openings are all examples of photo-initiated molecular machines that are at the core of energy conversion processes in biology, and all have been studied extensively with time-resolved spectroscopic methods. The methods and instrumentation described here should permit detailed molecular movies at the single bond level and with time resolution well below single vibrations in these molecules. Pre-alignment or orientation of the initial state using strong laser fields or other methods could also improve the measurement fidelity.

The scattering momentum available with our source energy and gas cell geometry is a limitation in this method. Future higher energy x-ray FELs could increase the fidelity and resolution of molecular movies. Likewise, the method is not restricted to long x-ray pulse duration, and could be used equally well with sub-femtosecond x-ray pulses. Enhanced harmonic radiation from FEL undulators could also be used.

We wish to acknowledge useful discussions with Ryan Coffee, Markus Guehr, Lucas Zipp, Andreas Kaldun, Jerry Hastings, Kelly Gaffney, Bob Schoenlein, and David Reis in the preparation of this paper. This research is supported through the Stanford PULSE Institute, SLAC National Accelerator Laboratory by the U.S. Department of Energy, Office of Basic Energy Sciences, Atomic, Molecular, and Optical Science Program. Use of the Linac Coherent Light Source (LCLS), SLAC National Accelerator Laboratory, is supported by the U.S. Department of Energy, Office of Science, Office of Basic Energy Sciences under Contract No. DE-AC02-76SF00515.

---

\* J.M. Glownia and A. Natan contributed equally to this work.

- [1] M. Trigo, M. Fuchs, J. Chen, M. P. Jiang, M. Cammarata, S. Fahy, D. M. Fritz, K. Gaffney, S. Ghimire, A. Higginbotham, S. L. Johnson, M. E. Kozina, J. Larsson, H. Lemke, A. M. Lindenberg, G. Ndabashimiye, F. Quirin, K. Sokolowski-Tinten, C. Uher, G. Wang, J. S. Wark, D. Zhu, and D. A. Reis, *Nature Physics* **9**, 790 (2013).
- [2] C. Kupitz, S. Basu, I. Grotjohann, R. Fromme, N. A. Zatsepin, K. N. Rendek, M. S. Hunter, R. L. Shoeman, T. A. White, D. Wang, D. James, J.-H. Yang, D. E. Cobb, B. Reeder, R. G. Sierra, H. Liu, A. Barty, A. L. Aquila, D. Deponte, R. A. Kirian, S. Bari, J. J. Bergkamp, K. R. Beyerlein, M. J. Bogan, C. Caleman, T.-C. Chao, C. E. Conrad, K. M. Davis, H. Fleckenstein, L. Galli, S. P. Hau-Riege, S. Kassemeyer, H. Laksmono, M. Liang, L. Lomb, S. Marchesini, A. V. Martin, M. Messerschmidt, D. Milathianaki, K. Nass, A. Ros, S. Roy-Chowdhury, K. Schmidt, M. Seibert, J. Steinbrener, F. Stellato, L. Yan, C. Yoon, T. A. Moore, A. L. Moore, Y. Pushkar, G. J. Williams, S. Boutet, R. B. Doak, U. Weierstall, M. Frank, H. N. Chapman, J. C. H. Spence, and P. Fromme, *Nature* **513**, 261 (2014).
- [3] M. Miniti, J. Budarz, A. Kirrander, J. Robinson,

D. Ratner, T. Lane, D. Zhu, J. Gownia, M. Kozina, H. Lemke, M. Sikorski, Y. Feng, S. Nelson, K. Saita, B. Stankus, T. Northey, J. Hastings, and P. Weber, *Physical Review Letters* **114**, 255501 (2015).

[4] J. Kupper, S. Stern, L. Holmegaard, F. Filsinger, A. Rouze, A. Rudenko, P. Johnsson, A. V. Martin, M. Adolph, A. Aquila, S. Bajt, A. Barty, C. Bostedt, J. Bozek, C. Caleman, R. Coffee, N. Coppola, T. Delmas, S. Epp, B. Erk, L. Foucar, T. Gorkhov, L. Gumprecht, A. Hartmann, R. Hartmann, G. Hauser, P. Holl, A. Hmke, N. Kimmel, F. Krasniqi, K.-U. Khnel, J. Maurer, M. Messerschmidt, R. Moshammer, C. Reich, B. Rudek, R. Santra, I. Schlichting, C. Schmidt, S. Schorb, J. Schulz, H. Soltau, J. C. Spence, D. Starodub, L. Strder, J. Thgersen, M. J. Vrakking, G. Weidenpointner, T. A. White, C. Wunderer, G. Meijer, J. Ullrich, H. Stapelfeldt, D. Rolles, and H. N. Chapman, *Physical Review Letters* **112**, 083002 (2014).

[5] M. Ben-Nun, J. Cao, and K. R. Wilson, *The Journal of Physical Chemistry A* **101**, 87438761 (1997).

[6] J. Cao and K. R. Wilson, *The Journal of Physical Chemistry A* **102**, 9523 (1998), <http://dx.doi.org/10.1021/jp982054p>.

[7] S. Bratos, F. Mirloup, R. Vuilleumier, and M. Wulff, *The Journal of Chemical Physics* **116**, 10615 (2002).

[8] N. E. Henriksen and K. B. Møller, *The Journal of Physical Chemistry B* **112**, 558 (2008), pMID: 18052363, <http://dx.doi.org/10.1021/jp075497e>.

[9] U. Lorenz, K. B. Møller, and N. E. Henriksen, *Phys. Rev. A* **81**, 023422 (2010).

[10] A. Debnarova, S. Techert, and S. Schmatz, *The Journal of Chemical Physics* **133**, 124309 (2010).

[11] G. Dixit, O. Vendrell, and R. Santra, *Proceedings of the National Academy of Sciences* **109**, 1163611640 (2012).

[12] M. Ben-Nun, T. J. Martnez, P. M. Weber, and K. R. Wilson, *Chemical Physics Letters* **262**, 405414 (1996).

[13] M. Woerner, F. Zamponi, Z. Ansari, J. Dreyer, B. Freyer, M. Prmont-Schwarz, and T. Elsaesser, *The Journal of Chemical Physics* **133**, 64509 (2010).

[14] M. J. J. Vrakking and T. Elsaesser, *Nature Photonics* **6**, 645647 (2012).

[15] D. A. Reis and A. M. Lindenberg, "Ultrafast x-ray scattering in solids," in *Light Scattering in Solid IX*, Topics in Applied Physics, edited by M. Cardona and R. Merlin (Springer Berlin Heidelberg, 2006) p. 371422.

[16] M. Chollet, R. Alonso-Mori, M. Cammarata, D. Damiani, J. Defever, J. T. Delor, Y. Feng, J. M. Gownia, J. B. Langton, S. Nelson, and et al., *Journal of Synchrotron Radiation* **22**, 503507 (2015).

[17] J. M. Budarz, M. P. Miniti, D. V. Cofer-Shabica, B. Stankus, A. Kirrander, J. B. Hastings, and P. M. Weber, *Journal of Physics B: Atomic, Molecular and Optical Physics* **49**, 34001 (2016).

[18] S. Herrmann, S. Boutet, B. Duda, D. Fritz, G. Haller, P. Hart, R. Herbst, C. Kenney, H. Lemke, M. Messerschmidt, et al., *Nuclear Instruments and Methods in Physics Research Section A: Accelerators, Spectrometers, Detectors and Associated Equipment* **718**, 550 (2013).

[19] H. Chen, L. Fang, V. Tagliamonti, and G. N. Gibson, *Physical Review A* **84**, 43427 (2011).

[20] D. W. Broege, R. N. Coffee, and P. H. Bucksbaum, *Physical Review A* **78**, 35401 (2008).

[21] F. Rosca-Pruna and M. J. J. Vrakking, *The Journal of Chemical Physics* **116**, 65796588 (2002).

[22] F. Rosca-Pruna and M. J. J. Vrakking, *Physical Review Letters* **87**, 153902 (2001).